

See discussions, stats, and author profiles for this publication at: <https://www.researchgate.net/publication/329677496>

# High permittivity ceramics improve the transmit field and receive efficiency of a commercial extremity coil at 1.5 Tesla

Article in *Journal of Magnetic Resonance* · December 2018

DOI: 10.1016/j.jmr.2018.12.013

CITATIONS

19

READS

134

5 authors, including:



**Irena Zivkovic**

Eindhoven University of Technology

29 PUBLICATIONS 247 CITATIONS

[SEE PROFILE](#)



**Alexey Slobzhanyuk**

ITMO University

157 PUBLICATIONS 3,216 CITATIONS

[SEE PROFILE](#)



**Elizaveta Nenasheva**

Ceramics Co.Ltd

81 PUBLICATIONS 1,223 CITATIONS

[SEE PROFILE](#)



**Andrew Webb**

Leiden University Medical Centre

568 PUBLICATIONS 18,580 CITATIONS

[SEE PROFILE](#)

Some of the authors of this publication are also working on these related projects:



Smart table for wireless power transfer [View project](#)



Metasurfaces for MRI [View project](#)



# High permittivity ceramics improve the transmit field and receive efficiency of a commercial extremity coil at 1.5 Tesla

Irena Zivkovic<sup>a</sup>, Wouter Teeuwisse<sup>a</sup>, Alexey Slobozhanyuk<sup>b</sup>, Elizaveta Nenasheva<sup>c</sup>, Andrew Webb<sup>a,\*</sup>

<sup>a</sup> C.J. Gorter Center for High Field MRI, Department of Radiology, Leiden University Medical Center, Leiden, the Netherlands

<sup>b</sup> Department of Nanophotonics and Metamaterials, ITMO University, Saint Petersburg, Russia

<sup>c</sup> Giricond Research Institute, Ceramics Co., Ltd., Saint Petersburg, Russia

## ARTICLE INFO

### Article history:

Received 26 May 2018

Revised 7 December 2018

Accepted 14 December 2018

Available online 15 December 2018

### Keywords:

High permittivity materials

Transmit efficiency

Receive sensitivity

Reduced SAR

1.5 T MRI

## ABSTRACT

**Objective:** The purpose of this work is to investigate the use of ceramic materials (based on BaTiO<sub>3</sub> with ZrO<sub>2</sub> and CeO<sub>2</sub>-additives) with very high relative permittivity ( $\epsilon_r \sim 4500$ ) to increase the local transmit field and signal-to-noise ratio (SNR) for commercial extremity coils on a clinical 1.5 T MRI system.

**Methods:** Electromagnetic simulations of transmit efficiency and specific absorption rate (SAR) were performed using four ferroelectric ceramic blocks placed around a cylindrical phantom, as well as placing these ceramics around the wrist of a human body model. Results were compared with experimental scans using the transmit body coil of the 1.5 T MRI system and an eight-element extremity receive array designed for the wrist. SNR measurements were also performed for both phantom and in vivo scans.

**Results:** Electromagnetic simulations and phantom/in vivo experiments showed an increased in the local transmit efficiency from the body coil of  $\sim 20$ – $30\%$ , resulting in an  $\sim 50\%$  lower transmit power level and a significant reduction in local and global SAR throughout the body. For in vivo wrist experiments, the SNR of a commercial eight-channel receive array, integrated over the entire volume, was improved by  $\sim 45\%$  with the ceramic.

**Conclusion:** The local transmit efficiency as well as the SNR can be increased for 1.5 T extremity MRI with commercial array coils by using materials with very high permittivity.

© 2018 The Authors. Published by Elsevier Inc. This is an open access article under the CC BY-NC-ND license (<http://creativecommons.org/licenses/by-nc-nd/4.0/>).

## 1. Introduction

High permittivity materials (HPMs), which can be somewhat loosely defined as being engineered to have a relative permittivity ( $\epsilon_r$ ) higher than naturally-occurring substances such as water, have been developed to improve image and spectroscopic quality in a number of application areas of magnetic resonance. Aqueous suspensions of calcium titanate ( $\epsilon_r \sim 110$  at 298 MHz) were initially developed to increase the homogeneity of the transmit field for neuroimaging at 7 T [1], and have been used in a number of different applications at 7 T [2–8] and 3 T [6]. Increasing the relative permittivity using suspensions of barium titanate ( $\epsilon_r \sim 300$  at 298 MHz) [9,10] allows one to concentrate the transmit field more locally for specific applications such as inner ear imaging [11] at 7 T, or to extend applications to lower field strengths. Realizable values of  $\epsilon_r$  for water-based suspensions of metal titanates can

be extended to  $\sim 500$  either by compression [12] or the use of ceramic beads [13]. In order to reach higher values (and also lower losses) the density of the material must be increased [14]. Materials with relative permittivity values close to 1000 have been used in 7 T phosphorus spectroscopy [15] (Larmor frequency  $\sim 120$  MHz) and 3 T spine imaging [16]. To date the highest permittivity materials used in MRI have been reported by Rupprecht et al. [17] who used specialized ceramics based on lead zirconate titanate,  $\text{Pb}(\text{Zr}_x\text{Ti}_{1-x})\text{O}_3$  (PZT) at the morphotropic phase boundary. In their work a “soft” PZT was synthesized with a donor dopant to give a relative permittivity of 3300 (at 64 MHz). The authors showed significant increases in the local transmit efficiency and SNR at both 3 T and 1.5 T.

The main mechanism for increasing the transmit efficiency in the presence of dielectric material is related to the existence of dielectric displacement currents in material which produce secondary magnetic fields (Ampere’s law):

$$\nabla \times B = \mu(J_c + J_d) = \mu(\sigma E + j\omega\epsilon_0\epsilon_r E)$$

\* Corresponding author at: C.J. Gorter Center for High Field MRI, Department of Radiology, Leiden University Medical Centre, Albinusdreef 2, 2333 ZA Leiden, the Netherlands.

E-mail address: [a.webb@lumc.nl](mailto:a.webb@lumc.nl) (A. Webb).

The total current consists of two components – conductive current  $J_c$  and dielectric displacement current  $J_d$ . The field produced by dielectric displacement currents increases with frequency and the relative permittivity of the material. There is an optimal value of  $\epsilon_r$  for a given frequency which produces the maximum effect when the secondary field is superimposed on the primary one. The optimal  $\epsilon_r$  depends on the geometry of the dielectric pad and on the Larmor frequency. If the permittivity is increased beyond this value then wave effects occur inside the dielectric material which can increase the inhomogeneity and decrease the efficiency of the overall transmit field [9].

In this paper, we propose and evaluate both theoretically and experimentally a ferroelectric material based on  $\text{BaTiO}_3$  (with  $\text{ZrO}_2$  and  $\text{CeO}_2$ -additives) with an  $\epsilon_r \sim 4500$  for scanning extremities at 1.5 T. This very high value of the relative permittivity allows a further reduction in size of the HPMs compared to those shown by Rupprecht et al. [17]. These types of materials were originally designed for the design of ceramic capacitances and microwave devices operated by an electric field, e.g. modulators, filters, and phase-shifters [18,19]. High values of relative permittivity and low dielectric losses in barium titanate based ceramics can be achieved by using additives of cerium and zirconium oxides that shift the Curie temperature and blur the phase transition. This material exists in a paraelectric phase, i.e. it is a ferroelectric with a Curie point below room/body (operating) temperature with a spontaneous dielectric polarization below its Curie temperature  $T_c$ . Electromagnetic simulations were performed and experimental data acquired on both phantoms and human volunteers.

## 2. Methods

### 2.1. Material preparation

High permittivity blocks ( $71 \times 57 \times 13$  mm) were prepared as follows. Pre-synthesized  $\text{BaTiO}_3$  (HPBT-1) (Fuji Titanium Industry Co., Japan) with a Ba/Ti molar ratio of 0.996 and high purity  $\text{ZrO}_2$  and  $\text{CeO}_2$ -additives were mixed in a vibration mill for 3 h. Samples of the required geometrical shape and size were prepared by hydraulic pressing; a 10% solution of polyvinyl alcohol was used as a binder. The samples were sintered for three hours in an air atmosphere at a temperature of 1340 °C in an electric chamber furnace until there was zero water absorbance and a porosity less than 4% was obtained. In order to measure the electrical properties disc-shaped samples were covered with a silver-containing dope burnt-in at a temperature of  $840 \pm 20$  °C.

### 2.2. Material characterization

Scattering parameter ( $S_{11}$ ) measurements were performed with an unmatched pick up loop on a Vector Network Analyzer (VNA). The lowest resonant frequency, corresponding to the  $\text{TE}_{018}$  mode, of each block was recorded in order to measure the high frequency relative permittivity of the material by comparison with the value obtained from electromagnetic simulations (see below). The magnetic susceptibility of the ceramic was measured with a superconducting quantum interference device (SQUID) magnetometer (Quantum Design, MPMS XL).

### 2.3. Electromagnetic simulations

EM simulations were performed in CST Microwave Studio 2016 (CST Studio Suite, Computer Simulation Technology, Darmstadt, Germany). The CST eigenmode solver was used to confirm the relative permittivity by calculating the frequency of the  $\text{TE}_{018}$  mode.

In all other simulations the frequency domain solver was used to calculate the transmit ( $B_1^+$ ) field and SAR for the phantom and in vivo scans. The transmit coil was modelled as a 598 mm diameter and 536 mm long 32-leg high-pass birdcage (matching the physical construction of the 1.5 T body coil) driven by ideal voltage sources to produce a circularly-polarized transmission field. For phantom simulations, each of the two phantoms was modeled as a 60 mm diameter cylinder, length 180 mm, with relative permittivity  $\epsilon = 61$  and conductivity  $\sigma = 0.86$  S/m. For in vivo simulations the Gustav voxel body model (ITIS Foundation, Switzerland) [20] was used. For these latter simulations the smallest cell size was 0.8 mm and total number of cells was 8.2 million.

### 2.4. MRI data acquisition

All MRI measurements were performed on a Philips Ingenia 1.5 T system. The body coil (see simulation parameters) was used for transmission in all scans. Experiments were performed on healthy volunteers: written consent was obtained from all volunteers and all experiments followed protocols approved by the local medical ethics committee. For the phantom experiments two phantoms (water doped with copper sulphate to reduce the  $T_1$  value) were placed close to the centre of the magnet, at the same position in the z-direction. One phantom had four ceramic blocks placed symmetrically around its diameter. The relative  $B_1^+$  transmit and  $B_1^-$  receive fields with and without the ceramic blocks were estimated using a low tip angle gradient echo sequence with  $\text{TR} = 3.8$  ms,  $\text{TE} = 1.82$  ms,  $\text{FA} = 1^\circ$ , slice thickness = 7 mm, data matrix =  $64 \times 64$  and number of slices = 39 using the body coil for both transmit and receive. Since the  $B_1^+$  transmit and  $B_1^-$  receive fields are essentially identical at 1.5 T, the relative  $B_1^+$  of the transmit coil with and without the ceramic blocks was simply calculated as the square root of the image intensities. The  $B_1^+$  maps were also calculated by using a dual TR method. The sequence used was 3D GRE sequence with the following parameters  $\text{TR}_1/\text{TR}_2 = 5.7/35.7$  ms,  $\text{TE} = 1.68$  ms,  $\text{FA} = 15^\circ$ , number of slices = 39, slice thickness = 5 mm and the body coil was used for both transmit and receive.

For estimation of the SNR under realistic scanning conditions a commercial eight-channel wrist receive array (Philips) was used. The eight-channel array consists of three axially-oriented columns of coils with two, three and two rectangular elements, respectively, and one element which is present in the top flap which folds over the top of the wrist and is secured with a velcro strap: each element has linear dimensions of approximately 6 cm. In one experiment the ceramic blocks were placed around the phantom inside the array coil, in the other four equivalently-sized foam spacers were used. The SNR was calculated by repeating a multi-slice gradient echo sequence with  $\text{TR} = 40$  ms,  $\text{TE} = 4$  ms, flip angle  $45^\circ$ , and slice thickness 10 mm: twenty experiments were performed and the SNR calculated on a pixel-by-pixel basis as the ratio of the mean value to the standard deviation of the signal intensity over all of the images [21]. Separate power optimizations were performed for the experiments with and without blocks.

For in vivo comparisons, in one experiment four high permittivity blocks were assembled around the wrist of a healthy volunteer positioned inside the commercial eight-channel wrist receive coil, and for the other the same foam spacers were used as for the phantom experiments. Wrist images with and without the blocks were obtained using a clinical protocol including a  $T_1$ -weighted turbo spin echo (TSE) sequence with  $\text{TR} = 776$  ms,  $\text{TE} = 18$  ms,  $\text{FA} = 90^\circ$ , slice thickness = 2.5 mm, data matrix =  $512 \times 512$  and number of slices = 20.

### 3. Results

The lowest measured resonant frequency of the block (using an unmatched pickup loop), corresponding to the  $TE_{01}$  mode, was 92 MHz. Adjusting the permittivity in the eigenmode solver of the CST simulation software to match this frequency confirmed that  $\epsilon_r = 4500$ , i.e. the relative permittivity at 63.8 MHz is almost identical to that at 1 MHz. The conductivity of the material was estimated as  $\sigma = 1.79$  S/m by measuring the quality factor of the ceramic block at this lowest resonant frequency. This corresponds to  $\tan \delta \sim 0.1$  (at 63.8 MHz), which is in line with other very high permittivity materials [16,17].

The value of the volume magnetic susceptibility measured with the SQUID magnetometer was  $+8.8 \times 10^{-7}$  cgs. For comparison the value of air is  $+3.6 \times 10^{-7}$  cgs, and so we do not expect to see any significant effects on even relatively long echo time gradient echo images (this was confirmed at both 1.5 T and 3 T). To place in con-

text, materials such as nickel, often used in plating electronic components, which are known to produce image artefacts have magnetic susceptibilities more than eight orders of magnitude larger than the ceramic.

The measured reflection coefficient of the coil loaded with a human arm with and without blocks did not show significant changes, i.e. the noise is dominated by the combined loss of the arm and coil, with no additional losses introduced by the blocks. The measured  $S_{11}$  of all channels at 64 MHz was between  $-10.9$  and  $-11.6$  dB.

Fig. 1 (a) and (b) show the simulated  $B_1^+$  map for the two cylindrical phantoms placed vertically and horizontally, respectively, on the patient table with four ceramic blocks placed around the phantom on the left. The  $B_1^+$  maps were normalized to 1 W of input power. The results show that the presence of the high permittivity ceramic blocks increased the  $B_1^+$  field in the region surrounded by the blocks by  $\sim 18\%$  when the phantoms were placed vertically and by  $\sim 33\%$  for phantoms placed horizontally. The factor-of-two

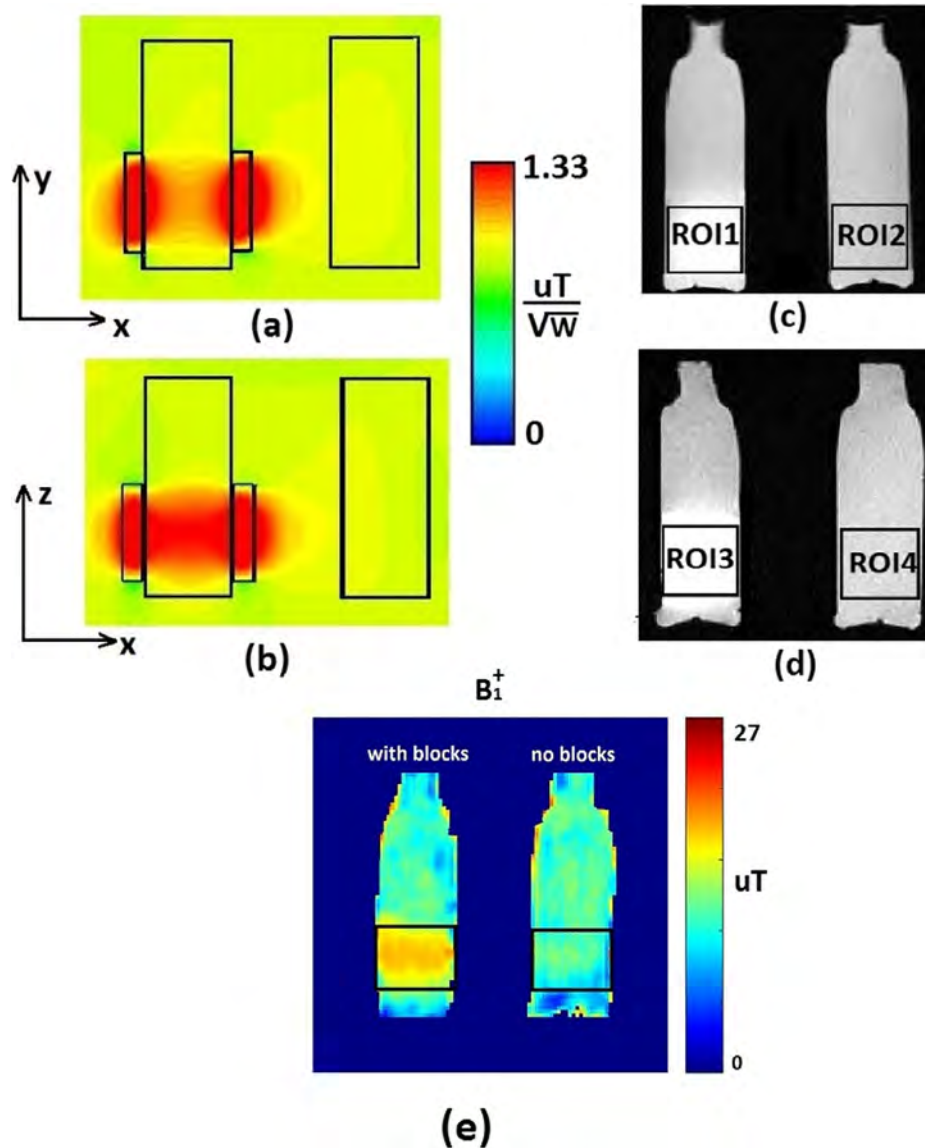


**Fig. 1.** Simulated  $B_1^+$  efficiency map at 63.8 MHz of two cylindrical phantoms placed (a) vertically and (b) horizontally at the centre of the magnet: a 32 channel birdcage body coil was used for RF transmission. The  $B_1^+$  map is scaled to 1 W input power. The phantom on the left had four high permittivity blocks placed symmetrically around it. (c) and (d) Measured low tip angle images of two phantoms with blocks placed around the phantom, (c) vertically and (d) horizontally with the body coil used for both transmit and receive. Regions of interest (ROIs) used to calculate the SNR are indicated by the black rectangles. (e) Measured  $B_1^+$  map (in  $\mu T$ ) of two bottles with and without blocks placed horizontally (same as in (b)) in the center of the magnet.

difference nicely illustrates the effect arising from the direction of the induced displacement currents as discussed by Rupprecht et al. [17]. Fig. 1(c) and (d) show corresponding low tip angle gradient echo images of the two phantoms scanned simultaneously, in both vertical and horizontal orientations. The regions of interest (ROIs) used to compare the signal intensities are marked with black rectangles. The signal intensity averaged over ROI 1 (Fig. 1 (c)) of the left phantom is enhanced by  $\sim 30\%$  compared to the signal intensity averaged over ROI 2, which corresponds to an increase in  $B_1^+$  (and also  $B_1^-$ ) of  $\sim 15\%$ . The signal intensity averaged over ROI 3 (Fig. 1 (d)) of the left phantom is enhanced by  $\sim 80\%$  compared to the signal intensity averaged over ROI 4, which corresponds to an increase in  $B_1^+$  (and also  $B_1^-$ ) of  $\sim 34\%$ . The measured  $B_1^+$  map of the setup that corresponds to the horizontally placed bottles with and without blocks (Fig. 1 (e)) shows an average increase in  $B_1^+$  field in a phantom with blocks of  $\sim 34\%$  compared to the phantom with-

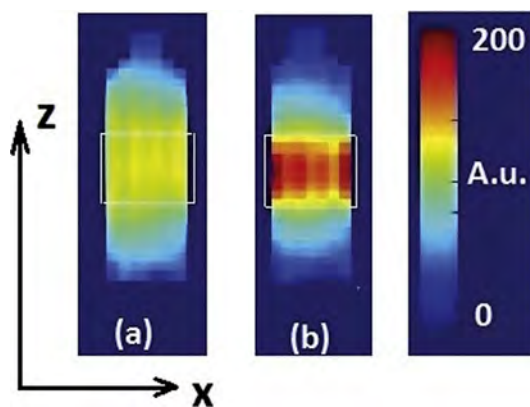


Fig. 2. Measured SNR on the bottle phantom without blocks (a) and with blocks (b) in arbitrary units (AU). The regions inside white squares were compared. The body coil was used for transmit and an eight channel array in reception.

out blocks, which coincides with the estimation concluded from the Fig. 1 (d).

Fig. 2 shows one gradient echo image used for the SNR measurements on the phantom with and without blocks (measured separately) placed inside the commercial eight channel extremity receive array. Separate power calibration was performed for the two experiments to ensure that the same excitation tip angle was used in both cases. The transmitted power level with the blocks was  $\sim 50\%$  lower than the power level of the scan of phantom without blocks. Using the repeated measurement method described previously the SNR increase in the ROI (white rectangle) was  $\sim 45\%$  compared to the phantom without blocks.

Fig. 3 shows the results of EM simulations using the voxel body model of the  $B_1^+$  field normalized per square root of input power, and the 10 g averaged SAR with and without blocks placed around the wrist. Fig. 3(b) shows that the  $B_1^+$  efficiency increased by  $\sim 30\%$  averaged over the volume of the wrist surrounded by the ceramic blocks. This is a similar number to the phantom simulations shown in Fig. 2, and corresponds to being able to use  $\sim 50\%$  less power. Fig. 3(c) shows the corresponding 10 g averaged SAR calculations, which show a decrease in the 10 g averaged SAR over the entire body. Interestingly, the highest 10 g averaged SAR is found in the wrist since it is located very close to the high electric field area of the transmit body coil. A large reduction in the 10 g averaged SAR in the wrist is also evident.

Fig. 4(a) shows a photograph of the experimental setup used for scanning the wrist in vivo. Four blocks of ceramic were placed around the radiocarpal joint of the wrist. Fig. 4 (b) and (c) show  $T_1$ -weighted TSE images from our standard clinical imaging protocol without and with ceramic blocks. Using the automatic power calibration protocol for the clinical system the image with ceramic blocks required 40% lower power than the image without blocks. This lower power corresponds to an  $\sim 25\%$  increase in  $B_1^+$  field efficiency which corresponds well with the simulation results shown in Fig. 3. Using the power calibration values, as would be the case

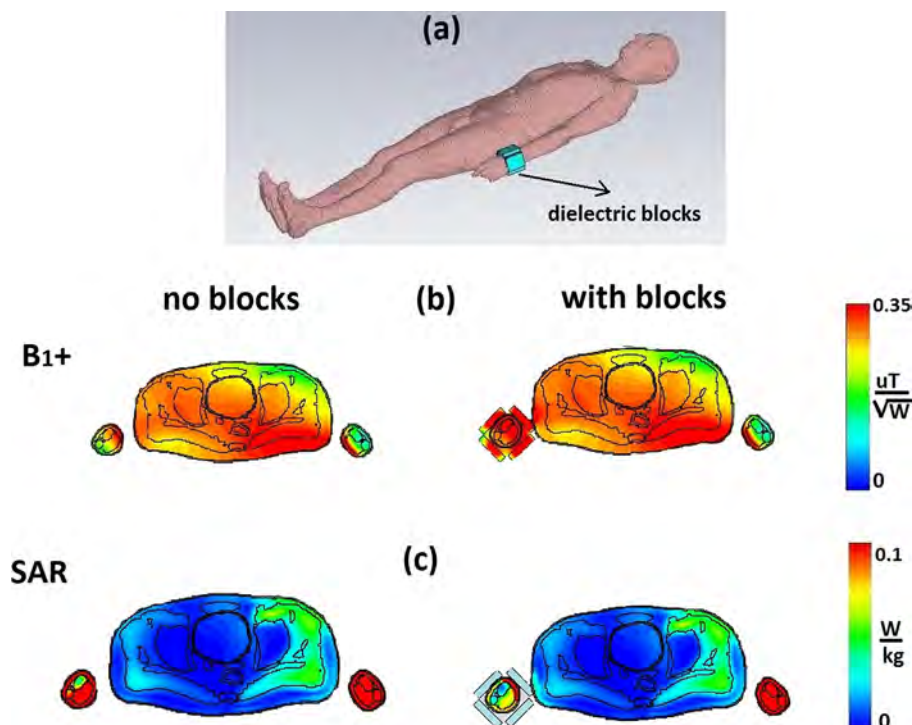
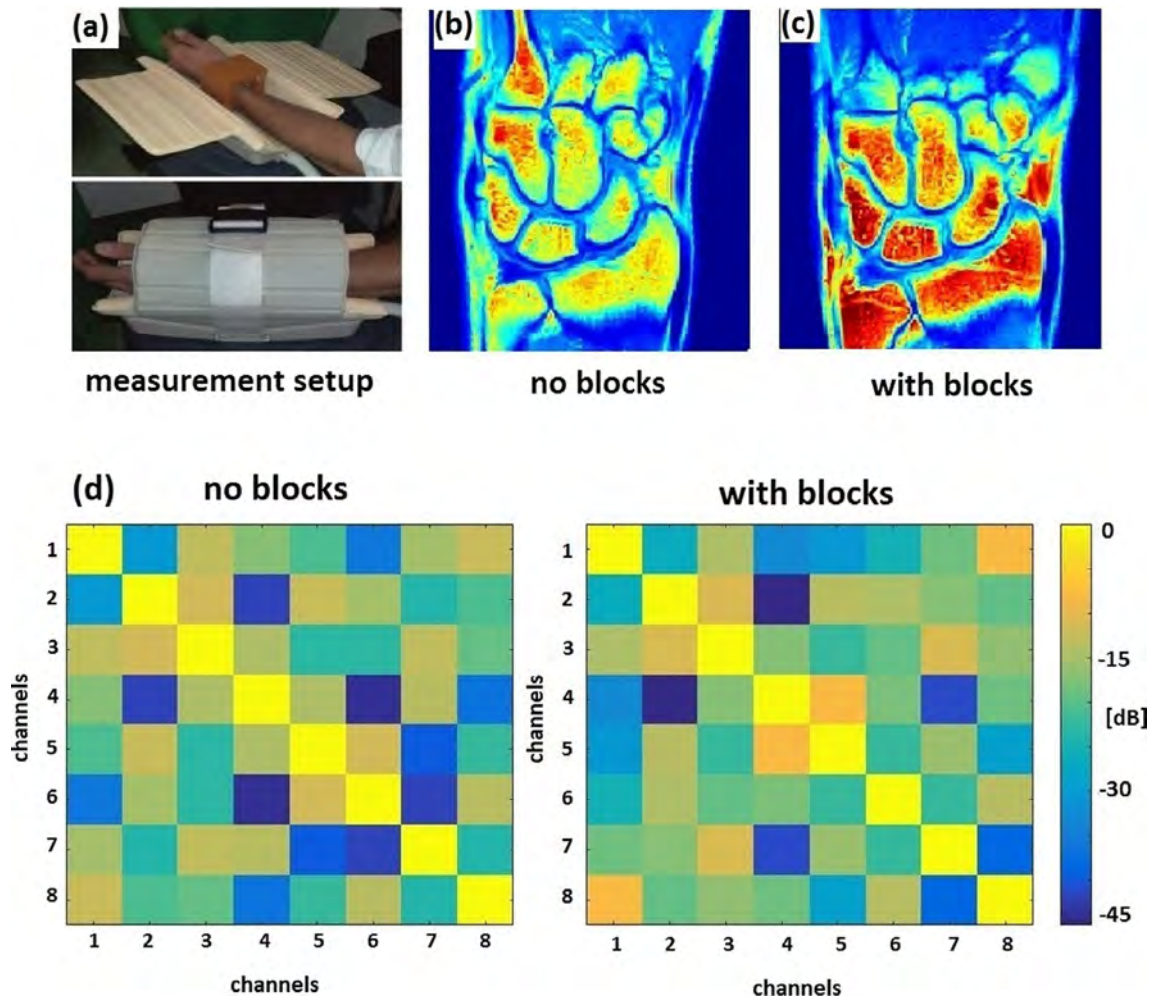


Fig. 3. (a) Simulated setup – four high permittivity ceramic blocks were placed around wrist of the voxel model Gustav. (b) Simulated  $B_1^+$  efficiency per square root of accepted power without and with blocks. (c) Simulated  $SAR_{10g}$  average without and with blocks.





**Fig. 4.** (a) Photographs of the in vivo experimental setups with a volunteer, ceramic blocks placed around the wrist and the commercial eight-channel receive array coil. (b)  $T_1$ -weighted wrist images without blocks, and (c) with blocks. The power level from the transmitter coil was 40% lower in the case of scanning the wrist with blocks compared to without blocks. The SNR is approximately 50% higher with the blocks over an ROI comprising the entire imaged volume. (d) Noise correlation matrices of the receive coil without and with blocks.

for clinical scanning, the image with ceramic blocks in Fig. 4(c) shows  $\sim 50\%$  higher signal intensity compared to the image without blocks. This increase in SNR results primarily from the increased local  $B_1^+$ , as has been reported by previous authors [17]. The measured noise correlation matrices of the receive coil without and with blocks are shown in Fig. 4(d). No significant changes in coupling coefficients were observed in measurements without and with blocks.

#### 4. Discussion and conclusion

This work has shown that materials with very high  $\epsilon_r$  ( $\sim 4500$ ) can be used to increase both the transmit and receive sensitivities at 1.5 T. These results are similar to those shown by previous authors [17], with the higher  $\epsilon_r$  in this paper allowing smaller ceramic blocks to be used for extremity imaging in which signal enhancements were seen throughout the entire imaging region-of-interest. Experimental results showed good agreement with electromagnetic simulations, indicating that significant reductions in power transmission from the body coil can be achieved.

The results presented here, and elsewhere, can be considered in the framework of ultimate intrinsic signal to noise (UISNR), introduced by the group of Atalar [22,23]. Previous authors have shown that at 1.5 Tesla loop coils produce only divergence-free current

patterns and so large arrays of such loop coils can approach the UISNR [24]. These latter results show that 95% of the UISNR can be attained at the centre of a spherical sample using only 8 loops at 1.5 Tesla; however, the SNR at the periphery of the imaging field-of-view is only 50% of the UISNR. In order to achieve 95% of the UISNR over the entire volume, a very large number of appropriately-sized, close-fitting loops need to be used: commercially these types of coils are simply not produced or even exceed the channel count of most systems. Our results show that we recover a significant percentage of the UISNR at the surface of the imaging field-of-view by using high permittivity materials for the situation of eight loops. Mechanistically, the basic principles of how dielectric materials can increase the SNR has been described recently [25]. The authors described the manipulation of the RF transmit and receive field by combining a surface loop coil with high permittivity dielectric material. One of the major conclusions of that study is that the effect of the high permittivity material is to increase the effective number of coils, which would of course more closely approach the UISNR. We have also performed essentially an identical set of simulations at 1.5 Tesla, with an identical conclusion.

Further increases in  $\epsilon_r$  would enable even thinner elements to be used, and so it is interesting to monitor the literature for materials with extremely high permittivities. New materials such as cal-

cium copper titanate (CCTO) have what is termed a “giant permittivity.”  $\text{CaCu}_3\text{Ti}_4\text{O}_{12}$  has been reported to have a dielectric constant at 1 kHz of about 12,000 that is nearly constant from room temperature to 300 °C [26]. The cubic structure of the general class of materials  $\text{ACu}_3\text{Ti}_4\text{O}_{12}$  (where A represents a metal) is related to that of perovskites such as calcium titanate, except the fact that the  $\text{TiO}_6$  octahedra are tilted [26,27]. However, these classes of material have relatively high loss tangents reported, up to 0.3. Even higher permittivity values have been reported for lanthanum strontium nickelates [28,29], although there is relatively little information on losses at frequencies relevant for MRI. As discussed previously, there is an optimal value of  $\epsilon_r$  which produces the maximum effect when superimposed on the original field [9].

While such increases in SNR are very useful clinically, another important future application may be in cases where the imaging ROI is different from the location of a medical implant. Common examples include patients with cardiac stents who require imaging of local areas of the spinal column or the extremities. In this case the power delivered to the entire body during the scan can be reduced due to the increase of the transmit efficiency, and this leads to a reduced 10-g averaged SAR, allowing a scan to be performed under normal scanning conditions rather than having to use a reduced SAR mode. Our results at 1.5 T are in line with electromagnetic simulations performed by Yu et al. [30] at 3 T, in which HPMS could be placed around the imaging region-of-interest in order to concentrate the local transmit field produced by the body coil, resulting in a reduction in the required power transmitted by the body coil for a given image contrast, and an associated reduction in the SAR averaged over 1 g of tissue next to a pacemaker lead by almost 75% [30]. This approach could also potentially be combined with other promising approaches such as parallel RF transmission [31,32], or using coil geometries which are specifically designed to reduce the electric fields in pre-determined areas [33,34].

## Authors' contributions

Study conception and design: Zivkovic, Teeuwisse, Webb.  
Materials: Slobozhanyuk, Nenasheva.  
Simulations and acquisition of data: Zivkovic, Teeuwisse, Webb.  
Analysis and interpretation of data: Zivkovic, Teeuwisse, Webb.  
Manuscript writing: Zivkovic, Teeuwisse, Webb, Slobozhanyuk, Nenasheva.

## Compliance with ethical standards

Funding: European Research Council Advanced Grant (670629 NOMA MRI).

Conflict of interest: The authors declare that they have no conflict of interest.

Ethical Approval: All studies were approved by the medical ethics committee of the Leiden University Medical Center.

## Acknowledgments

This work was supported by a European Research Council Advanced Grant ERC 670629 NOMA MRI (IZ, WT, AW) and the Ministry of Education and Science of the Russian Federation ZadanieNo. 3.2465.2017/4.6 (APS).

## References

- [1] K. Haines, N.B. Smith, A.G. Webb, New high dielectric constant materials for tailoring the B-1(+) distribution at high magnetic fields, *J. Magn. Reson.* 203 (2010) 323–327.

- [2] C. Lemke, A. Hess, S. Clare, V. Bachtir, C. Stag, P. Jezard, U. Emir, Two-voxel spectroscopy with dynamic B0 shimming and flip angle adjustment at 7 T in the human motor cortex, *NMR Biomed.* 28 (2015) 852–860.
- [3] B. Schaller, L. Xin, K. O'Brien, A.W. Magill, R. Gruetter, Are glutamate and lactate increases ubiquitous to physiological activation? A (1)H functional MR spectroscopy study during motor activation in human brain at 7 Tesla, *Neuroimage* 93 (Pt 1) (2014) 138–145.
- [4] K.R. O'Brien, A.W. Magill, J. Delacoste, J.P. Marques, T. Kober, H.P. Fautz, F. Lazeyras, G. Krueger, Dielectric pads and low- B1+ adiabatic pulses: complementary techniques to optimize structural T1 w whole-brain MP2RAGE scans at 7 tesla, *J. Magn. Reson. Imaging* 40 (2014) 804–812.
- [5] A.T. Vu, E. Auerbach, C. Lenglet, S. Moeller, S.N. Sotiropoulos, S. Jbabdi, J. Andersson, E. Yacoub, K. Ugurbil, High resolution whole brain diffusion imaging at 7 T for the Human Connectome Project, *Neuroimage* 122 (2015) 318–331.
- [6] Y. Wang, S. Moeller, X. Li, A.T. Vu, K. Krasileva, K. Ugurbil, E. Yacoub, D.J. Wang, Simultaneous multi-slice Turbo-FLASH imaging with CAIPIRINHA for whole brain distortion-free pseudo-continuous arterial spin labeling at 3 and 7 T, *Neuroimage* 113 (2015) 279–288.
- [7] A. Deistung, A. Schafer, F. Schweser, U. Biedermann, D. Gullmar, R. Trampel, R. Turner, J.R. Reichenbach, High-resolution MR imaging of the human Brainstem in vivo at 7 Tesla, *Front. Hum. Neurosci.* 7 (2013) 710.
- [8] A. Manoliu, G. Spinner, M. Wyss, D.A. Ettlin, D. Nanz, F.P. Kuhn, L.M. Gallo, G. Andreisek, Magnetic resonance imaging of the temporomandibular joint at 7.0 T using high-permittivity dielectric pads: a feasibility study, *Invest. Radiol.* 50 (2015) 843–849.
- [9] W.M. Teeuwisse, W.M. Brink, K.N. Haines, A.G. Webb, Simulations of high permittivity materials for 7 T neuroimaging and evaluation of a new barium titanate-based dielectric, *Magn. Reson. Med.* 67 (2012) 912–918.
- [10] W.M. Teeuwisse, W.M. Brink, A.G. Webb, Quantitative assessment of the effects of high-permittivity pads in 7 Tesla MRI of the brain, *Magn. Reson. Med.* 67 (2012) 1285–1293.
- [11] W.M. Brink, A.M.A. van der Jagt, M.J. Versluis, B.M. Verbist, A.G. Webb, High permittivity dielectric pads improve high spatial resolution magnetic resonance imaging of the inner ear at 7 T, *Invest. Radiol.* 49 (2014) 271–277.
- [12] A.L. Neves, L. Leroi, Z. Raulison, N. Cochinaire, T. Letertre, R. Abdeddaim, S. Enoch, J. Wenger, J. Berthelot, A.L. Adenot-Engelvin, N. Mallejac, F. Mauconduit, A. Vignaud, P. Sabouroux, Compressed perovskite aqueous mixtures near their phase transitions show very high permittivities: new prospects for high-field MRI dielectric shimming, *Magn. Reson. Med.* 79 (2018) 1753–1765.
- [13] W. Luo, M.T. Lanagan, C.T. Sica, Y. Ryu, S. Oh, M. Ketterman, Q.X. Yang, C.M. Collins, Permittivity and performance of dielectric pads with sintered ceramic beads in MRI: early experiments and simulations at 3 T, *Magn. Reson. Med.* 70 (2013) 269–275.
- [14] W. Luo, J. Guo, C. Randall, M. Lanagan, Effect of porosity and microstructure on the microwave dielectric properties of rutile, *Mater. Lett.* 200 (2017) 101–104.
- [15] B.Y. Lee, X.H. Zhu, S. Rupprecht, M.T. Lanagan, Q.X. Yang, W. Chen, Large improvement of RF transmission efficiency and reception sensitivity for human in vivo P-31 MRS imaging using ultrahigh dielectric constant materials at 7 T, *Magn. Reson. Imaging* 42 (2017) 158–163.
- [16] K. Koolstra, P. Bornert, W. Brink, A. Webb, Improved image quality and reduced power deposition in the spine at 3 T using extremely high permittivity materials, *Magn. Reson. Med.* 79 (2018) 1192–1199.
- [17] S. Rupprecht, C.T. Sica, W. Chen, M.T. Lanagan, Q.X. Yang, Improvements of transmit efficiency and receive sensitivity with ultrahigh dielectric constant (uHDC) ceramics at 1.5 T and 3 T, *Magn. Reson. Med.* 79 (2018) 2842–2851.
- [18] E.A. Nenasheva, A.D. Kanareykin, N.F. Kartenko, A.I. Dedyk, S.F. Karmanenko, Ceramics materials based on (Ba, Sr)TiO<sub>3</sub> solid solutions for tunable microwave devices, *J. Electroceram.* 13 (2004) 235–238.
- [19] E.A. Nenasheva, N.F. Kartenko, I.M. Gaidamaka, O.N. Trubitsyna, S.S. Redozubov, A.I. Dedyk, A.D. Kanareykin, Low loss microwave ferroelectric ceramics for high power tunable devices, *J. Eur. Ceram. Soc.* 30 (2010) 395–400.
- [20] A. Christ, W. Kainz, E.G. Hahn, K. Honegger, M. Zefferer, E. Neufeld, W. Rascher, R. Janka, W. Bautz, J. Chen, B. Kiefer, P. Schmitt, H.P. Hollenbach, J.X. Shen, M. Oberle, D. Szczerba, A. Kam, J.W. Guag, N. Kuster, The Virtual Family-development of surface-based anatomical models of two adults and two children for dosimetric simulations, *Phys. Med. Biol.* 55 (2010) N23–N38.
- [21] O. Dietrich, J.G. Raya, S.B. Reeder, M.F. Reiser, S.O. Schoenberg, Measurement of signal-to-noise ratios in MR images: influence of multichannel coils, parallel imaging, and reconstruction filters, *J. Magn. Reson. Imaging* 26 (2007) 375–385.
- [22] E. Kopanoglu, V.B. Erturk, E. Atalar, Analytic expressions for the ultimate intrinsic signal-to-noise ratio and ultimate intrinsic specific absorption rate in MRI, *Magn. Reson. Med.* 66 (2011) 846–858.
- [23] O. Ocali, E. Atalar, Ultimate intrinsic signal-to-noise ratio in MRI, *Magn. Reson. Med.* 39 (1998) 462–473.
- [24] R. Lattanzi, G.C. Wiggins, B. Zhang, Q. Duan, R. Brown, D.K. Sodickson, Approaching ultimate intrinsic signal-to-noise ratio with loop and dipole antennas, *Magn. Reson. Med.* 79 (2018) 1789–1803.
- [25] M.V. Vaidya, C.M. Deniz, C.M. Collins, D.K. Sodickson, R. Lattanzi, Manipulating transmit and receive sensitivities of radiofrequency surface coils using shielded and unshielded high-permittivity materials, *Magn. Reson. Mater. Phys.* 31 (2018) 355–366.

- [26] M.A. Subramanian, D. Li, N. Duan, B.A. Reisner, A.W. Sleight, High dielectric constant in  $\text{ACu(3)Ti(4)O(12)}$  and  $\text{ACu(3)Ti(3)FeO(12)}$  phases, *J. Solid State Chem.* 151 (2000) 323–325.
- [27] A.G. Webb, Dielectric materials in magnetic resonance, *Concept Magn Reson. A* 38a (2011) 148–184.
- [28] S. Krohns, P. Lunkenheimer, C. Kant, A.V. Pronin, H.B. Brom, A.A. Nugroho, M. Diantoro, A. Loidl, Colossal dielectric constant up to gigahertz at room temperature, *Appl. Phys. Lett.* 94 (2009).
- [29] S. Krohns, P. Lunkenheimer, S. Meissner, A. Reller, B. Gleich, A. Rathgeber, T. Gaugler, H.U. Buhl, D.C. Sinclair, A. Loidl, The route to resource-efficient novel materials, *Nat. Mater.* 10 (2011) 899–901.
- [30] Z.D. Yu, X.G. Xin, C.M. Collins, Potential for high-permittivity materials to reduce local SAR at a pacemaker lead tip during MRI of the head with a body transmit coil at 3T, *Magn. Reson. Med.* 78 (2017) 383–386.
- [31] C.E. McElcheran, B.S. Yang, K.J. Anderson, L. Golestanirad, S.J. Graham, Parallel radiofrequency transmission at 3 tesla to improve safety in bilateral implanted wires in a heterogeneous model, *Magn. Reson. Med.* 78 (2017) 2406–2415.
- [32] C.E. McElcheran, B.S. Yang, K.J.T. Anderson, L. Golestanirad, S.J. Graham, Investigation of parallel radiofrequency transmission for the reduction of heating in long conductive leads in 3 tesla magnetic resonance imaging, *Plos One* 10 (2015).
- [33] Y. Eryaman, B. Akin, E. Atalar, Reduction of implant RF heating through modification of transmit coil electric field, *Magn. Reson. Med.* 65 (2011) 1305–1313.
- [34] Y. Eryaman, E.A. Turk, C. Oto, O. Algin, E. Atalar, Reduction of the radiofrequency heating of metallic devices using a dual-drive birdcage coil, *Magn. Reson. Med.* 69 (2013) 845–852.